Norwalk Virus Assembly and Stability Monitored by Mass Spectrometry

Shoemaker, Glen K.; van Duijn, Esther; Crawford, Sue E.; Uetrecht, Charlotte; Baclayon, Marian; Roos, Wouter H.; Wuite, Gijs J. L.; Estes, Mary K.; Prasad, B. V. Venkataram; Heck, Albert J. R.

Published in:
Molecular & Cellular Proteomics

DOI:
10.1074/mcp.M900620-MCP200

Publication date:
2010

Norwalk Virus Assembly and Stability Monitored by Mass Spectrometry*[S]

Glen K. Shoemaker‡§, Esther van Duijn‡§, Sue E. Crawford¶, Charlotte Uetrecht‡§, Marian Baclayon‖, Wouter H. Roos‖, Gijs J. L. Wuite‖, Mary K. Estes¶, B. V. Venkataram Prasad**, and Albert J. R. Heck‡§‡‡

Viral capsid assembly, in which viral proteins self-assemble into complexes of well defined architecture, is a fascinating biological process. Although viral structure and assembly processes have been the subject of many excellent structural biology studies in the past, questions still remain regarding the intricate mechanisms that underlie viral structure, stability, and assembly. Here we used native mass spectrometry-based techniques to study the structure, stability, and assembly of Norwalk virus-like particles. Although detailed structural information on the fully assembled capsid exists, less information is available on potential capsid (dis)assembly intermediates, largely because of the inherent heterogeneity and complexity of the disassembly pathways. We used native mass spectrometry and atomic force microscopy to investigate the (dis)assembly of the Norwalk virus-like particles as a function of solution pH, ionic strength, and VP1 protein concentration. Native MS analysis at physiological pH revealed the presence of the complete capsid ($T = 3$) consisting of 180 copies of VP1. The mass of these capsid particles extends over 10 million Da, ranking them among the largest protein complexes ever analyzed by native MS. Although very stable under acidic conditions, the capsid was found to be sensitive to alkaline treatment. At elevated pH, intermediate structures consisting of 2, 4, 6, 18, 40, 60, and 80 copies of VP1 were observed with the $VP1_{60}$ (3.36-MDa) and $VP1_{80}$ (4.48-MDa) species being most abundant. Atomic force microscopy imaging and ion mobility mass spectrometry confirmed the formation of these latter midsize spherical particles at elevated pH. All these VP1 oligomers could be reversely assembled into the original capsid ($VP1_{180}$). From the MS data collected over a range of experimental conditions, we suggest a disassembly model in which the $T = 3$ $VP1_{180}$ particles dissociate into smaller oligomers, predominantly dimers, upon alkaline treatment prior to reassembly into $VP1_{60}$ and $VP1_{80}$ species. ***Molecular & Cellular Proteomics 9: 1742–1751, 2010.***

Accounting for most cases of non-bacterial gastroenteritis, the norovirus represents an important human pathogen (1, 2). It is the most predominant pathogen within the family Caliciviridae, which also includes *Sapovirus*, *Vesivirus*, and *Lagovirus* (3). The prototypical strain of the genus *Norovirus* is the Norwalk virus. It is a small (7.7-kb genome) non-enveloped, single-stranded RNA virus. Its genome contains three open reading frames, encoding for the major capsid protein (VP1), the minor capsid protein (VP2), and a non-structural polyprotein (4, 5). VP1 forms homodimers, and the mature Norwalk virus capsids ($T = 3$) are composed of 90 VP1 dimers (6, 7) and possibly a few copies of VP2 that are thought to stabilize the icosahedral structure as well as affect the expression of VP1 (7, 8). Because of a lack of suitable animal models or *in vitro* cell culture systems, structural studies so far have been largely focused on recombinant norovirus-like particles (rNVLPs),[1] which are spontaneously assembled during the expression of recombinant VP1 and VP2 in insect cells (5). Importantly, these empty noninfectious particles have been demonstrated to be morphologically and antigenically similar to the genuine virion (9).

The rNVLPs have been studied extensively using X-ray crystallography and electron microscopy (EM), which have provided a detailed image of the intact capsid, revealing the $T = 3$ icosahedral organization (6, 9–11). The VP1 monomer structure is principally composed of two domains, an S domain consisting of the 225 N-terminal residues and a C-terminal P domain. In the intact capsid, the S domain forms a contiguous protein shell with a diameter of ~30 nm, whereas the P domain forms prominent protrusions, which give the rNVLPs a diameter of ~40 nm. A remarkable feature of the rNVLPs is that a single protein is responsible for directing capsid assembly and host interactions. The rNVLPs thus represent a simple model to study the assembly of icosahedral viruses. Although the requirements for capsid assembly have

From the ‡Biomolecular Mass Spectrometry and Proteomics Group, Bijvoet Center for Biomolecular Research and Utrecht Institute for Pharmaceutical Sciences, Utrecht University, 3584 CH Utrecht, The Netherlands, §Netherlands Proteomics Center, ¶Molecular Virology and Microbiology and **Biochemistry and Molecular Biology, Baylor College of Medicine, Houston, Texas 77030, and ‖Natuur-en Sterrenkunde, Vrije Universiteit, 1081 HV Amsterdam, The Netherlands

Received, December 21, 2009, and in revised form, April 1, 2010
Published, MCP Papers in Press, April 22, 2010, DOI 10.1074/mcp.M900620-MCP200

[1] The abbreviations used are: rNVLP, recombinant norovirus-like particle; AFM, atomic force microscopy; ccs, collision cross-section(s); HBV, hepatitis B virus; IMMS, ion mobility MS; VP, viral protein; mbar, millibars; EM, electron microscopy.

been investigated previously (7, 10), there is little information regarding intermediates along the (dis)assembly pathway. Obtaining such information can be quite difficult because of the inherent heterogeneity of capsid assembly. An emerging technique for interrogating such heterogeneous protein assemblies is native electrospray ionization mass spectrometry (ESI-MS).

Long regarded as a tool for small molecule analysis and more recently proteomics investigations, the utility of mass spectrometry in structural biology is increasingly applied and accepted (12–15). Native mass spectrometry exploits the gentle ionization conditions afforded by electrospray ionization to transfer intact non-covalently bound protein assemblies into the gas phase. Determining the mass of these complexes with high accuracy allows the oligomeric stoichiometry to be unambiguously deduced. Traditionally challenging targets for structural biology, including complexes in the megadalton range (15–17), heterogeneous or polydisperse assemblies (18, 19), and membrane-bound protein assemblies (20) can now be interrogated in this manner. Furthermore, selective dissociation of these assemblies in both the gas and solution phases allows the designation of subcomplexes, non-covalently bound species smaller than the original protein complex. Combining the knowledge obtained from such data provides information regarding subunit organization at both the architecture and subarchitecture level, allowing the generation of low resolution maps of the overall three-dimensional structure of protein complexes (21–23). Additional information can also be obtained through the combination of tandem MS techniques. CID, for example, can be used to selectively dissociate specific protein assemblies and thus provide information regarding the stability and aid in the assignment of stoichiometry for a given complex. Another tandem MS approach, ion mobility MS (IMMS), provides additional information regarding the shape of gaseous protein complexes. In IMMS, in addition to separation based on their mass-to-charge ratio, ions are also passed through an ion mobility cell with a counterflow of neutral background gas where they are separated based on their size and shape (13, 24).

The ability to perform mass measurements of intact viruses has been exploited by several groups but is often limited by mass resolution, which is impeded by the incomplete desolvation of the large protein assemblies during the ionization process. Siuzdak *et al.* (25) and Robinson and co-workers (26) pioneered the analyses of viruses using mass spectrometry. More recently Uetrecht *et al.* (15, 17) reported ESI-MS data on the hepatitis B virus (HBV) capsid. In these studies, sufficient mass resolution was obtained to determine the accurate mass and stoichiometry of the $T = 3$ and $T = 4$ HBV capsids despite their large mass of 3 and 4 million Da, respectively (15, 17). In addition to being able to measure the mass and stoichiometry of protein assemblies, the capacity of native MS to analyze simultaneously a heterogeneous population of assembly intermediates makes it a powerful technique to study virus assembly (27).

In the work described here, the disassembly of rNVLPs was monitored over a range of solution conditions using native ESI-MS, providing insights into their stability and factors that govern icosahedral assembly for this model calicivirus. Unraveling the details of these complex structures and the associated self-assembly pathways that lead to their efficient and precise construction may play an important role in the development of antiviral therapeutics and in the field of nanotechnology where there is much interest in the fundamentals of particle self-assembly.

EXPERIMENTAL PROCEDURES

Preparation of rNVLPs for ESI-MS Analysis—The native ESI-MS measurements were carried out using recombinant VP1, which was expressed in *Spodoptera frugiperda* (Sf9) cells using a baculovirus expression system and purified as described previously (9). Briefly, Sf9 cells were harvested 5–7 days after baculovirus infection and then purified using centrifugation with a CsCl gradient of 1.362 g/cm^3. The purified rNVLPs (400 μM VP1) were stored in water at 4 °C. For ESI-MS analysis, the rNVLPs were exchanged into an aqueous ammonium acetate buffer (50–500 mM) at various pH values using an Amicon Ultra 0.5-ml centrifugal filter (Millipore, Billerica, MA) with a molecular mass cutoff of 10 kDa. The pH of the aqueous ammonium acetate solution was adjusted by using an aqueous solution of either ammonia or acetic acid. All measurements at the different experimental conditions were repeated at least three times on different days. Additionally, results from two different preparations of reconstituted rNVLPs yielded consistent results.

Mass Spectrometry—High resolution and tandem mass spectra were recorded on a modified Q-ToF 1 instrument (Waters) in positive ion mode (28). To enhance the transmission of the large ions corresponding to rNVLPs, xenon, at a pressure of 2×10^{-2} mbar, was used in the collision cell (29). The voltages and pressures were also optimized for large non-covalent protein complexes (30). Briefly, the capillary and cone voltages were kept constant at 1450 and 165 V, respectively. The voltage before the collision cell was varied from 10 to 400 V but generally left at 50 V for the accumulation of native ESI mass spectra. Ions were introduced into the source under an elevated pressure of 10 mbar. Ion mobility measurements were performed on a Synapt HDMS (Waters) (31). To generate intact gas phase ions from large protein complexes in solution, the source was maintained at 6.1 mbar, and voltages of 1400 and 164 V were applied to the capillary and sample cone, respectively. Xenon was used as the background gas in the trap and transfer ion guides at a flow rate of 4 ml/min. The voltages in the trap and transfer were 20 and 25 V, respectively. The gas in the ion mobility cell was nitrogen at a flow rate of 25 ml/min and a ramped wave height of 10–30 V with a velocity of 250 m/s. Ramped wave heights were shown previously to provide better results for protein complexes in the megadalton range (17). Collision cross-sections (ccs) were determined from the measured drift times through calibration using proteins of known cross-sections as described previously (17, 32, 33). Denatured ESI-MS analysis of the VP1 monomers was performed on an LCT instrument (Waters). The performance of the instruments was tested with an aqueous CsI solution, and a calibration was applied where necessary. ESI tips were prepared in house from borosilicate glass tubes of 1.2-mm outer diameter and 0.68-mm inner diameter (World Precision Instruments, Sarasota, FL) by using a P-97 micropipette puller (Sutter Instruments, Novato, CA). The ESI tips were gold-coated using a Scancoat six Pirani 501 sputter coater (Edwards Laboratories, Milpitas, CA).

Atomic Force Microscopy—Atomic force microscopy (AFM) experiments were conducted in aqueous ammonium acetate solutions with

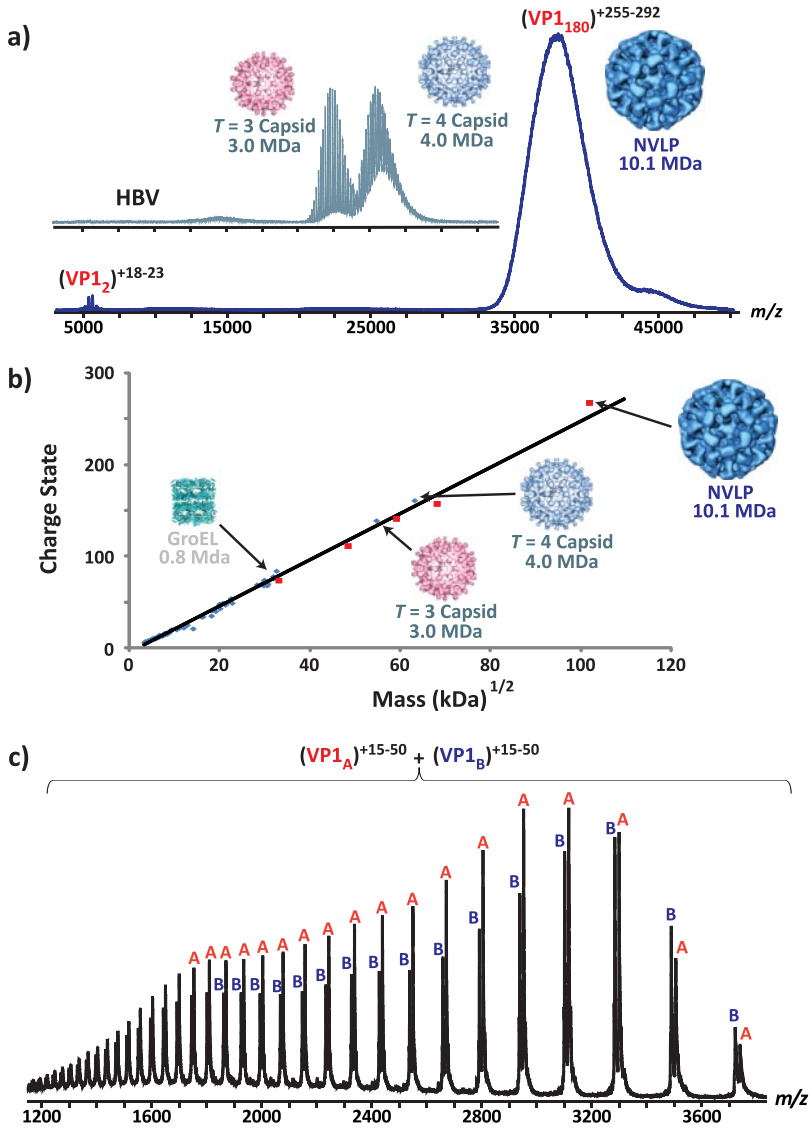

FIG. 1. **Native ESI-MS analysis of rNVLPs.** *a*, representative native ESI mass spectrum of an aqueous solution containing rNVLPs (30 μM VP1) in a 250 mM aqueous ammonium acetate buffer at pH 7. For comparison, a native ESI mass spectrum of the HBV capsid is also shown (15). *b*, a plot of charge state *versus* the square root of the mass for several macromolecular assemblies analyzed by ESI-MS (♦) (45), including the rNVLPs, VP1 oligomers ($VP1_{180}$, $VP1_{80}$, $VP1_{60}$, $VP1_{40}$, and $VP1_{18}$) (■), and the $T = 3$ and $T = 4$ HBV capsids (♦). *c*, denatured ESI mass spectrum obtained from a solution containing rNVLPs (16 μM VP1) in 20% (v/v) acetonitrile and 1% (v/v) formic acid, demonstrating the mass heterogeneity of the VP1 monomers. The individual charge states for $VP1_A$ and $VP1_B$ are labelled A or B, respectively.

a Nanotec Electronica (Madrid, Spain) instrument operating in jumping mode (34) using rectangular gold-coated cantilevers (Olympus, Zoeterwoude, The Netherlands) with a tip apex nominal value of <20 nm. The cantilevers were calibrated as described previously (35) and were found to have a spring constant of 0.052 ± 0.004 newton/m. Glass coverslips were cleaned by immersion in an 86% (v/v) ethanol solution saturated with KOH for 14 h. After being rinsed thoroughly with deionized water and left to dry, the coverslips were rendered hydrophobic by incubating them under a saturated hexamethyldisilazane (Fluka, Zwijndrecht, The Netherlands) vapor for 14 h (36). For imaging, a droplet containing VP1 (0.2–10 μM) in an aqueous ammonium acetate buffer (500 mM) at various pH values was placed on the hydrophobic glass coverslip and analyzed after a short (5-min) incubation.

RESULTS AND DISCUSSION

ESI-MS Analysis of rNVLPs—To first investigate whether the intact capsid can be detected using ESI-MS, the rNVLPs were analyzed at neutral pH, a condition that is known from previous EM studies to be favorable for the formation of intact capsid (7, 9). A mass spectrum at pH 7 in a 250 mM aqueous ammonium acetate buffer is presented in Fig. 1*a*. A broad distribution of ions is present in the high *m/z* region of the mass spectrum, corresponding to intact rNVLPs as well as a small amount of VP1 dimers (around *m/z* 5000). Because the individual charge states of the capsid ions are unresolved, the mass cannot be precisely assigned. Importantly, however, the ions corresponding to rNVLPs are detected in the expected region of the mass spectrum. To demonstrate this, an *inset* of two other virus capsids analyzed by ESI-MS is included in Fig. 1*a*. This spectrum corresponds to the two HBV capsids, which exhibit $T = 3$ and $T = 4$ symmetry, that possess masses of 3 and 4 MDa, respectively (15, 17). These data are also represented as a plot of charge state *versus* the square root of the mass for several protein and protein assemblies analyzed by ESI-MS that is expected to be linear according to the charge residue model for electrospray ioni-

zation (37, 38). As can be seen in Fig. 1*b*, the plot demonstrates excellent linearity, and the rNVLPs are detected around the expected charge state. With a mass of ~10.1 MDa, the rNVLPs are among the largest protein assemblies analyzed by native ESI-MS. We attempted to subject these capsid ions to high energy CID to enhance desolvation, but unfortunately, the individual charge states remained unresolved. At even higher voltages in the collision cell, dissociation of the capsid was observed that proceeded with the loss of VP1 monomers and concomitant high mass fragments, which could not be well resolved (data not shown).

To confirm the identity and homogeneity of the major capsid protein (VP1), the rNVLPs were also analyzed with ESI-MS under denaturing conditions. The rNVLPs were denatured in an acetonitrile/water solution that was acidified using formic acid (Fig. 1*c*). The denatured mass spectrum revealed the existence of two nearly equally abundant VP1 monomer species with masses of 56,077 ± 2 and 55,813 ± 2 Da, respectively. The relative abundance of each monomer was determined from Fig. 1*c*, and an average weighted monomer mass of 55,960 Da was used in all subsequent stoichiometry assignments for the VP1 oligomers. The two monomer species differ in mass by 264 Da, which is consistent with two methionine residues. Thus, the two co-existing VP1 monomer species likely arise from differences in post-translational methionine processing as there are three sequential methionines located at the VP1 N terminus. This mass heterogeneity in the VP1 monomers is an important contributing factor for the lack of charge state resolution for the rNVLP ions (Fig. 1*a*). Notably, similar heterogeneity in VP1 monomer species has been reported previously using SDS-PAGE (39). Absent from the mass spectra was the minor structural protein VP2. It was expected from previous experiments that a few copies of VP2 could be present per capsid, but no VP2 was detected in the denatured MS analysis or on the SDS-PAGE gels. Its precise stoichiometry and role in capsid assembly thus remain unclear.

Analysis of rNVLP Stability and (Dis)assembly Intermediates—The stability of rNVLPs over a range of solution conditions has been probed using EM and various spectroscopic techniques (7, 10). From this work, it was discovered that although the rNVLPs are stable under acidic conditions they are quite sensitive to even slightly alkaline treatment. Consistent with these previous studies, under acidic pH, ions corresponding exclusively to the intact capsid were observed in the mass spectrum (data not shown). Even at pH 2.5, intact rNVLPs dominated the spectrum, although some small VP1 oligomers, predominantly VP1 monomers and dimers, were also detected. Conversely, upon alkaline treatment, extensive capsid dissociation was observed. Representative mass spectra of the rNVLPs in a 250 mM ammonium acetate buffer over a pH range of 6–9 are given in Fig. 2. Additionally, the ion intensities for all species were summed for each solution pH and are represented in the bar graph included in Fig. 2. It

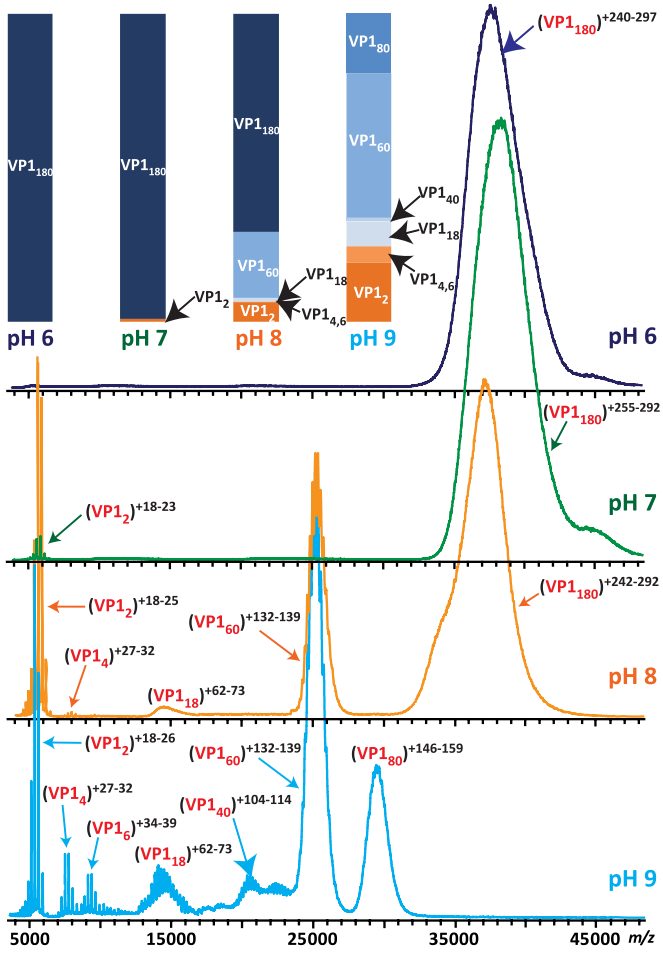

FIG. 2. **Stability of rNVLPs over a pH range of 6–9 monitored by native ESI-MS.** Mass spectra were obtained from aqueous solutions of the rNVLPs (30 μM VP1) in a 250 mM ammonium acetate buffer at the pH values indicated. The summed intensities for all observed VP1 oligomers at each pH are summarized in the bar graphs in the *upper left corner*.

should be noted that for all the spectra collected in Fig. 2 all other important variables such as VP1 concentration and ionic strength were kept constant. As can be seen in Fig. 2, at pH 8, extensive capsid dissociation was observed as VP1 dimers were quite abundant in the spectrum. Several (dis)assembly intermediates were also detected, consisting of 4, 6, 18, and 60 copies of VP1, with the $VP1_{60}$ species (3.4 MDa) being the most populated of the VP1 oligomers at this pH. Interestingly, smaller capsids were also reported in a previous EM study (39). These smaller particles possessed a diameter of around 25 nm and were speculated to be $T = 1$ particles made up of 60 copies of VP1. Thus, it appears that at this pH the intact capsid can disassemble, initially forming smaller VP1 oligomers, predominantly dimers. These small VP1 oligomers can then interact to reform higher order oligomers, predominantly $VP1_{60}$ at pH 8. For the norovirus, it has been suggested that in solution the VP1 dimers may exist in two distinct conformations and that the N terminus of VP1 acts as a switch to

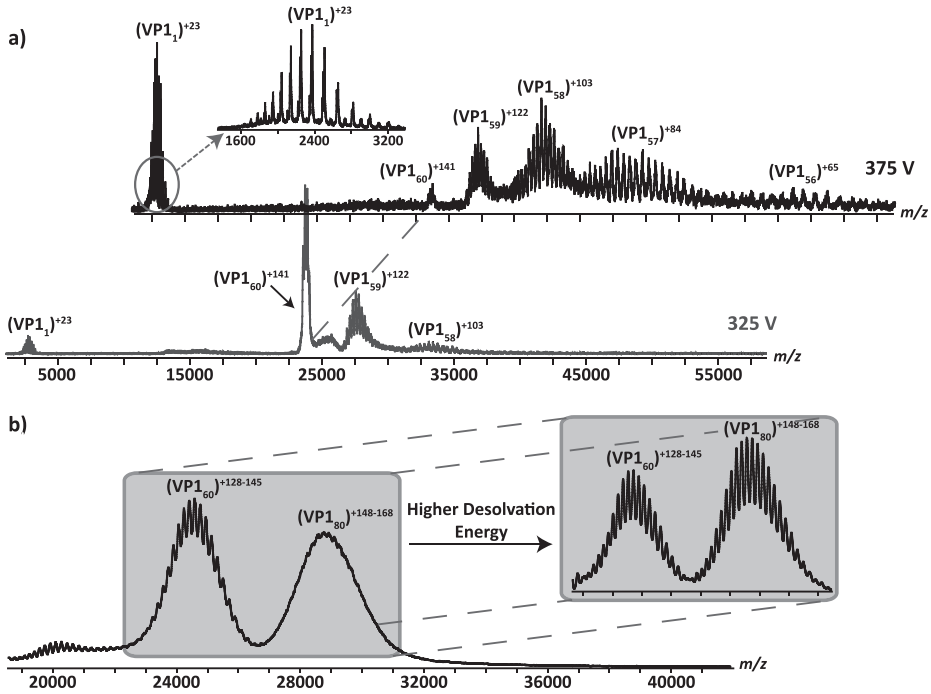

FIG. 3. **Illustrative ESI mass spectra demonstrating the identification of the higher order VP1 oligomers ($VP1_{60}$ and $VP1_{80}$).** *a*, representative CID mass spectra of isolated ions corresponding to $VP1_{60}$ excited with a voltage of 325 and 375 V before the collision cell. All CID spectra were obtained from aqueous solutions of the rNVLPs (30 μM VP1) in a 250 mM ammonium acetate buffer (pH 9). *b*, when selection of specific ions was not possible, as was the case for the high *m/z* $VP1_{80}$ ions, spectra were collected at a higher desolvation energy in the collision cell (200 V) to improve resolution and mass assignment.

distinguish between these two dimer conformations guiding $T = 3$ icosahedral assembly (11, 40). Thus, there are perhaps subtle pH-induced conformational changes within the VP1 dimers, affecting the switching mechanism and leading to the formation of alternate capsids with different symmetry and stoichiometry.

A further increase of the solution pH to 9 led to the complete loss of the full $VP1_{180}$ capsid and the formation of more midsize VP1 oligomers. At the low *m/z* region, a series of VP1 oligomers was observed: $VP1_2$, $VP1_4$, $VP1_6$, and a small amount of $VP1_8$ and $VP1_{10}$. In the higher *m/z* region, again the $VP1_{60}$ species was detected in high abundance. Additionally, VP1 oligomers consisting of 18, 40, and 80 copies of VP1 were observed. Of all the VP1 oligomers detected, the $VP1_{60}$, $VP1_{80}$, and $VP1_{18}$ are the most populated of the higher order species. Interestingly, Middaugh and co-workers (7) postulated that three larger oligomeric forms of VP1 may exist at alkaline pH based on fitting their dynamic light scattering data to a multimodal distribution. Using ESI-MS, we could directly observe these species and assign their stoichiometry. This demonstrates one of the strengths of an MS-based approach to study protein assemblies as it is possible to simultaneously detect all oligomers within a heterogeneous population.

To confirm the identity of these larger VP1 oligomers, ions corresponding to each species were selected in the quadrupole and subjected to high energy CID (Fig. 3). Representative CID spectra of the $VP1_{60}$ species are given in Fig. 3*a*. Dissociation proceeded by the sequential loss of highly charged VP1 monomers with at most four monomers being ejected at the highest collision voltage investigated (400 V). The series of high mass dissociation products differing by one VP1 monomer confirms the oligomeric state of the parent 60-mer. Unfortunately, $VP1_{80}$ ions could not be selected using the quadrupole mass filter for tandem mass spectrometry as their *m/z* value is above the limit for precursor ion selection. Instead, the ions were analyzed with a sufficiently high energy in the collision cell to improve desolvation of the high mass ions but not cause any fragmentation (*i.e.* 200 V in the collision cell). As can be seen in Fig. 3*b*, this greatly enhanced the resolution of the individual charge states, making the determination of the stoichiometry unambiguous. To further support the assignment of these stoichiometries, simulated mass spectra of the two VP1 oligomers were superimposed over the experimental mass spectra of the $VP1_{60}$ and $VP1_{80}$ at high desolvation energy (supplemental Fig. S1) and exhibited excellent agreement. Simulations of these spectra using other stoichiometries, for instance $VP1_{72}$ and $VP1_{84}$, which represent closely related and allowed icosahedral symmetries, clearly did not match the experimental data, thus confirming the stoichiometry of the $VP1_{80}$ species. The charge state distributions for the $VP1_{80}$ and $VP1_{60}$ oligomers were also assigned assuming a stoichiometry of ± 1 VP1 dimer (supplemental Tables S1 and S2). From supplemental Tables S1 and S2, it can be

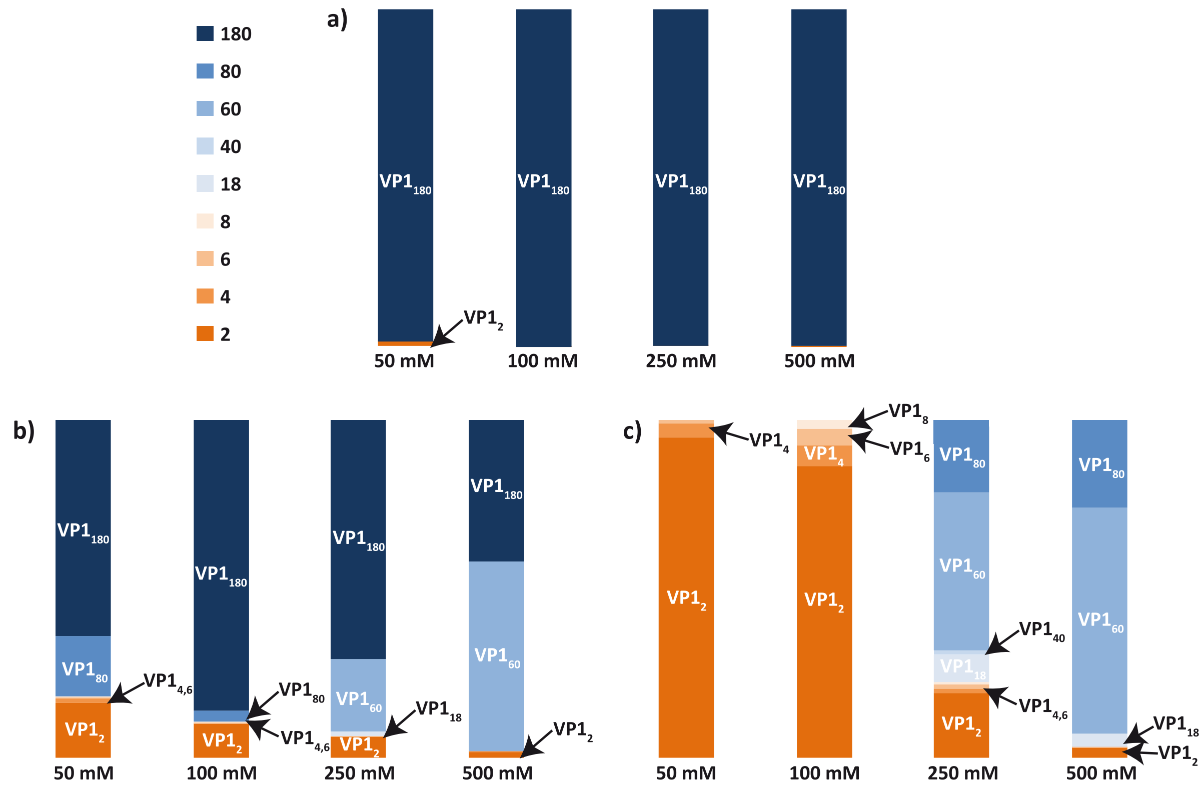

FIG. 4. **Effect of ionic strength on assembly of VP1 oligomers.** Assembly was monitored by ESI-MS at a solution pH of 7 (*a*), 8 (*b*), and 9 (*c*) under a range of ammonium acetate concentrations (50–500 mM).

seen that a stoichiometry of $VP1_{80}$ and $VP1_{60}$ represents the best fit to the experimental data. Additionally, the VP1 oligomers were included in the plot of the charge state *versus* the square root of mass (Fig. 1*b*). As can be seen in Fig. 1*b*, the VP1 oligomers of the different stoichiometries are all detected at the expected charge state.

It has been demonstrated for other icosahedral viruses, such as cowpea chlorotic mottle virus, that capsid assembly can also be influenced by ionic strength (41). To investigate the effect of ionic strength on the assembly of these VP1 oligomers, ESI-MS analysis was performed after dilution of the intact rNVLPs into various ammonium acetate buffers with a concentration range of 50–500 mM and a pH range of 7–9. The ion intensities for each VP1 oligomer were summed over all charge states at each solution composition and are summarized as bar graphs in Fig. 4. Over the entire range of ionic strength, ions corresponding to intact rNVLPs dominated the mass spectra at physiological pH (Fig. 4*a*) with only a small amount of VP1 dimer detected. Ionic strength had a much more significant effect under alkaline conditions. Here, extensive capsid dissociation was observed at each ionic strength value as evidenced by the formation of $VP1_2$ and other VP1 oligomers. Interestingly, at pH 8, the intact capsid was most abundant at an intermediate ionic strength of 100 mM (Fig. 4*b*). At this pH, the ionic strength also seems to govern which higher order VP1 oligomers are preferentially formed. Below 100 mM, a small amount of $VP1_{80}$, and no $VP1_{60}$ was detected. This is in sharp contrast to the results at higher ionic strengths in which significant $VP1_{60}$ was detected, and the $VP1_{80}$ was completely absent from the mass spectrum. At even lower ionic strengths (25 mM; data not shown), only small VP1 oligomers were detected. Another interesting trend at this pH is that the abundance of the $VP1_2$ decreased with increasing salt concentration with a concomitant increase in $VP1_{60}$ abundance. Thus, it appears that only above a certain threshold ionic strength can VP1 dimers reassemble into the $VP1_{60}$ species.

These trends are even more evident at pH 9 (Fig. 4*c*). At this pH, there was no intact $VP1_{180}$ at any of the ionic strengths investigated. As was observed at pH 8, at higher ionic strengths, there was an increasing propensity to form the high mass VP1 oligomers, such as $VP1_{60}$ and $VP1_{80}$, with a concomitant decrease in $VP1_2$ abundance. In fact, below a certain ionic strength threshold (100 mM), there were no higher order oligomers present as almost exclusively VP1 dimers were detected in the mass spectrum.

Another important factor in the formation of protein assemblies is the concentration of their protein building blocks. To investigate the effect of VP1 concentration on the assembly of these novel VP1 oligomers, serial dilutions of a VP1 stock solution (160 μM) in a 250 mM ammonium acetate buffer (pH 9) were made and analyzed by ESI-MS. Not surprisingly, it was found that at low concentrations of VP1 the large oligomers were very low in abundance, and $VP1_2$ was the dominant

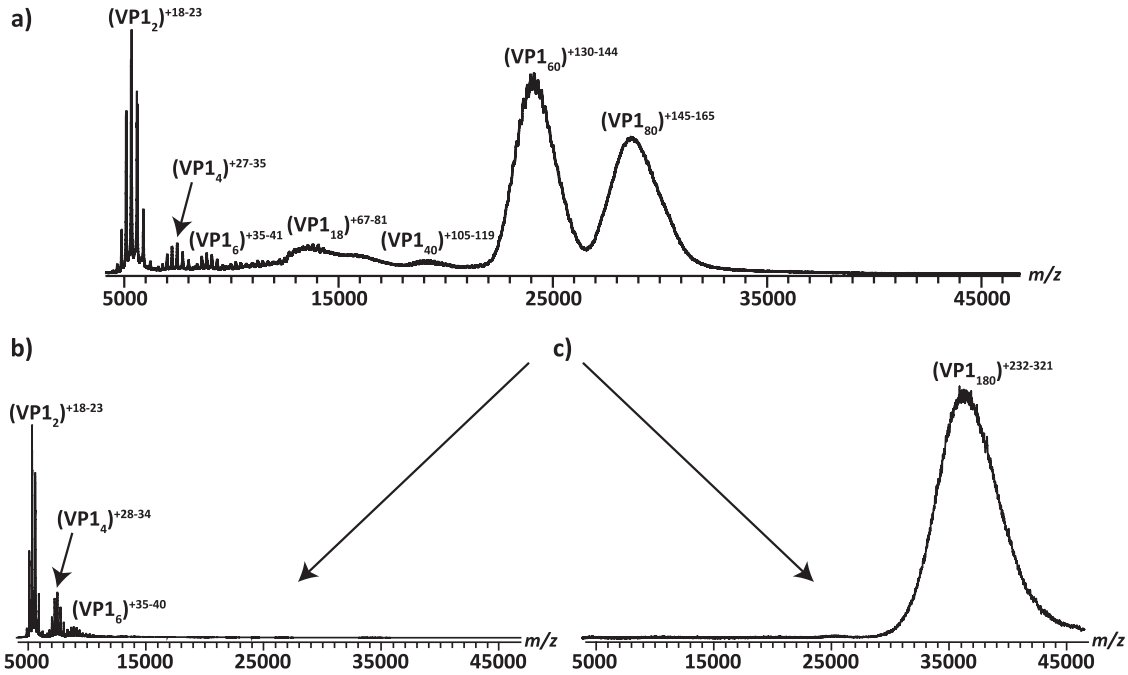

FIG. 5. **Representative ESI mass spectra demonstrating that assembly of various VP1 oligomers is reversible.** The solutions were prepared by diluting a stock solution of VP1 (160 μM) in a 250 mM ammonium acetate buffer (pH 9) 10-fold into 250 mM ammonium acetate buffer (pH 9) (*a*), 50 mM ammonium acetate buffer (pH 9) (*b*), and 250 mM ammonium acetate (pH 6) (*c*).

species in the spectrum (supplemental Fig. S2). With increasing VP1 concentration, $VP1_{60}$ and $VP1_{80}$ became more prevalent. Interestingly, the ratio of $VP1_{60}/VP1_{80}$ was also highly dependent on VP1 concentration. At a VP1 concentration of 23 μM (supplemental Fig. S2b), both oligomers were detected with similar intensities by ESI-MS. However, at the highest concentration investigated, 80 μM VP1, the $VP1_{80}$ species was ~8 times more abundant than the $VP1_{60}$ oligomer.

The assembly of these higher order VP1 oligomers was also found to be a reversible process (Fig. 5). In this experiment, the intact rNVLPs were first exchanged into conditions favorable for the formation of $VP1_{60}$ and $VP1_{80}$, namely 250 mM ammonium acetate (pH 9). An aliquot was removed from this stock solution, diluted into the same buffer, and analyzed by ESI-MS (Fig. 5*a*). From this stock solution, two additional aliquots were removed and diluted 10-fold into buffer with a different ionic strength or pH. One aliquot was diluted 10-fold into a lower ionic strength buffer (50 mM ammonium acetate) at the same pH prior to ESI-MS analysis (Fig. 5*b*). The corresponding mass spectrum is given in Fig. 5*b*. Consistent with Fig. 4*c*, the $VP1_{60}$ and $VP1_{80}$ species were not present because of the low ionic strength. Given that Fig. 5*b* was generated minutes after dilution into the low ionic strength buffer, the VP1 oligomers appear to be rapidly interconverting with the range of possible species being determined by the solution conditions (*i.e.* pH and ionic strength). The mass spectrum in Fig. 5*c* was generated by diluting the VP1 stock solution into a buffer of the same ionic strength but at pH 6. Under these conditions, intact rNVLPs are reassembled and dominate the mass spectrum. Thus, these experiments demonstrate the amazing ability of the VP1 to reversibly and rapidly form higher order structures depending upon the solution conditions. It has been recently suggested from molecular dynamics simulations of capsid assembly that strong reversible steps are essential to capsid formation as they diminish the effect of kinetic traps (42). This definitely appears to be the case for the rNVLPs and the VP1 oligomers described here and may explain why Norwalk virus is such a robust and environmentally persistent virion.

Structural Analysis of VP1 (Dis)assembly Intermediates—To confirm the presence of higher order VP1 oligomers (*i.e.* $VP1_{60}$ and $VP1_{80}$) and to gain insights into the shape of the various VP1 assemblies, AFM images were collected under the same solution conditions as used in the MS analysis. From the MS data, it was found that at a pH < 7 exclusively $VP1_{180}$ is present at all ionic strengths investigated (50–500 mM). Therefore, to confirm these results, AFM experiments were performed in buffers containing VP1 in a 500 mM ammonium acetate buffer at pH 6. Fig. 6 summarizes the height distribution of the imaged particles. A representative AFM image and height profile for one of the imaged $T = 3$ particles is included as an *inset*. Importantly, the particles were found to be spherical and to possess an average diameter of 40 $\pm$ 3 nm, which is in excellent agreement with the expected value of 38 nm for $VP1_{180}$ obtained from EM and X-ray crystallographic studies (6).

Next, we sought to obtain images of the intermediate VP1 assemblies, namely $VP1_{60}$ and $VP1_{80}$. From the MS data, it is

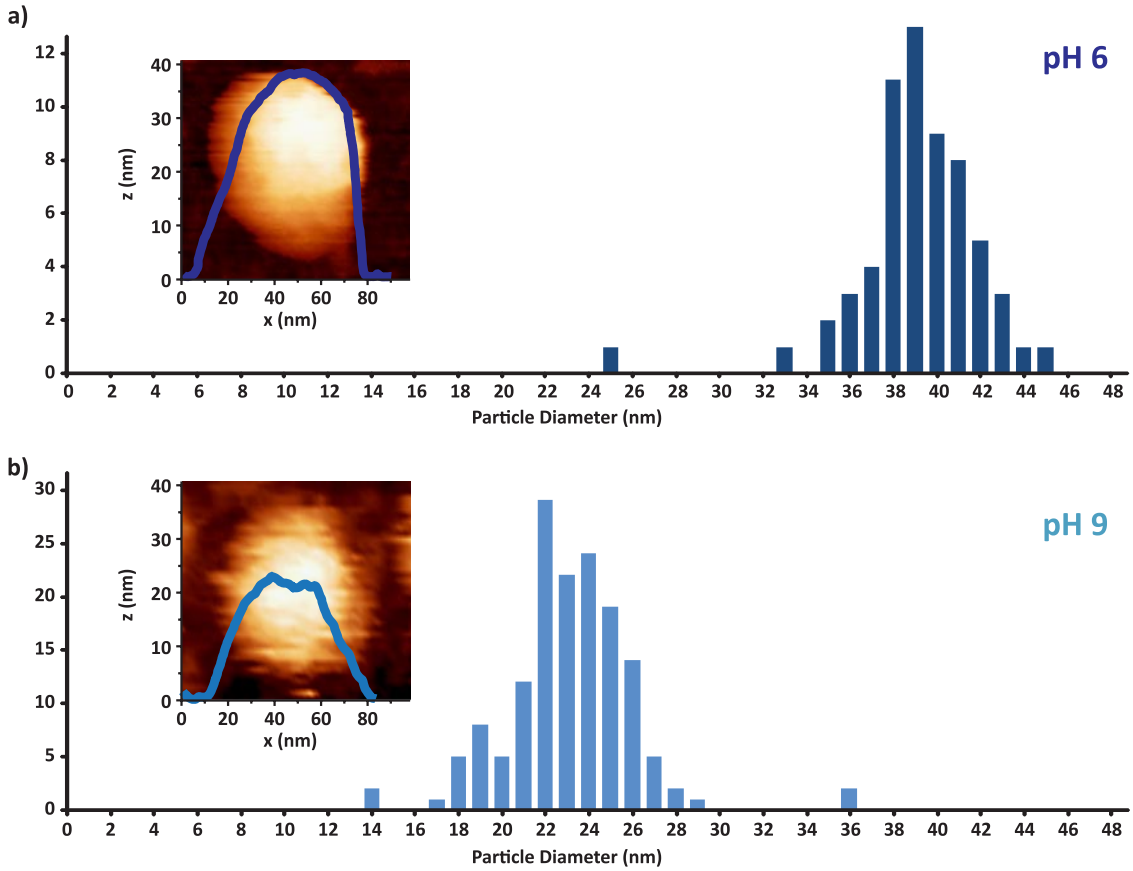

FIG. 6. **AFM imaging of rNVLPs and VP1 oligomers.** Particle size distribution histograms constructed from AFM data obtained for rNVLPs incubated in a 500 mM ammonium acetate buffer at pH 6 (*a*) and pH 9 (*b*) are shown. Representative AFM images and height profiles of the $VP1_{180}$ (*a*) and $VP1_{60}$ (*b*) are also included as *insets*. Imaging of the particles at pH 9 was difficult, possibly as a result of improper attachment. However, to allow comparison of the results at pH 6 and pH 9, similar hydrophobic surfaces were used in both experiments.

clear that the formation of both of these assemblies requires a high pH and a high ionic strength (Fig. 4*c*). Thus, VP1 was analyzed by AFM in a 500 mM ammonium acetate buffer at pH 9 (Fig. 6*b*). Consistent with the MS data, no $VP1_{180}$ particles were detected, and a broad distribution of smaller particles was present. Interestingly, the particles were spherical, suggesting that these smaller VP1 oligomers are indeed capsids of various stoichiometries and symmetries. The most abundant of these particles was a distribution of species around 22 nm. Under these conditions, it was found from MS that the most abundant VP1 oligomer was $VP1_{60}$. Combining information regarding stoichiometry obtained from MS with the structural data afforded by AFM provides strong evidence that the $VP1_{60}$ oligomer is a spherical capsid with $T = 1$ icosahedral symmetry. Additional support for this claim is provided by previous EM measurements, which, as mentioned earlier, also observed a $T = 1$ capsid with a diameter of 23 nm (39). Even more intriguing is the $VP1_{80}$ oligomer. Although most of the particles possess diameters of around 23 nm, there were some larger species detected in the AFM analysis likely corresponding to $VP1_{80}$. However, because of their low abundance, it is difficult to make any definitive conclusions regarding the morphology of the $VP1_{80}$ species. It is interesting to note that at this concentration of VP1 (10 μM) and at this solution composition, high ionic strength, and high pH, very little $VP1_{80}$ was detected by ESI-MS as well (supplemental Fig. S2). From the MS data, a higher VP1 concentration should lead to the formation of more $VP1_{80}$. It is difficult to perform the AFM analysis at such high VP1 concentrations because the glass plate becomes overcrowded with particles, precluding the height measurements of individual particles. Importantly, AFM experiments at higher VP1 concentrations yielded a distribution of particles with higher diameters that is consistent with the MS results.

To gain further structural insights into these VP1 oligomers, particularly the $VP1_{80}$ species, all oligomers were interrogated using IMMS. In IMMS, the mobility of ions through a pressurized tube is measured from which information may be gathered about the ccs of the ions, which may be used to obtain low resolution structural information about the species, like volume/shape/conformation, as reviewed recently (43). The experimentally determined ccs for the $VP1_{180}$, $VP1_{80}$, and $VP1_{60}$ oligomers are plotted in Fig. 7 *versus* their mass (in MDa). Interestingly, the measured ccs of rNLVP oligomers

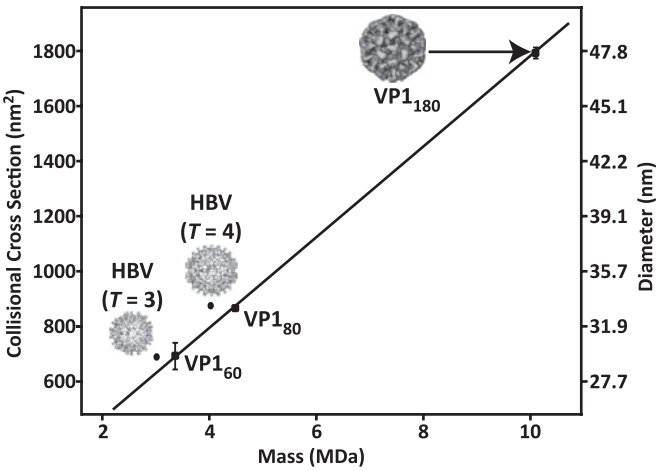

FIG. 7. **Size and shape of rNVLPs and VP1 oligomers determined by IMMS.** A plot of the calibrated ccs (nm^2) for the fully assembled rNVLPs and VP1 (dis)assembly intermediates (■) *versus* mass (MDa) is shown. For each species, the ccs increased linearly with mass, suggesting that these species adopt a similar hollow geometry. Included on the plot are values obtained for the HBV (●) capsid obtained previously (17). The diameters for each species, assuming a spherical geometry, are also included.

follow a linear trend and increase with mass, suggesting that these assemblies possess a similar (viral shell-like) geometry. Also included in the plot are ccs for the two morphologies observed for the HBV capsids reported previously (17). In this work, it was demonstrated by IMMS that the HBV capsids retain most likely a hollow spherical geometry upon transfer to the gas phase and throughout the IMMS analysis. As can be seen in Fig. 7, the HBV capsids follow the same linear increase in ccs with mass observed for the VP1 oligomers, suggesting that also all observed rNVPL stoichiometries (*i.e.* $VP1_{60}$, $VP1_{80}$, and $VP1_{180}$) have also adopted a hollow, closed geometry. This result is consistent with the AFM images and previous EM measurements that indicate that the $VP1_{60}$ and $VP1_{180}$ adopt a spherical icosahedral geometry. Most interestingly, the $VP1_{80}$ species fits on the same trend line; thus, it appears that the $VP1_{80}$ also adopts a closed, hollow geometry as opposed to an extended intermediate along the pathway to the full $T = 3$ $VP1_{180}$ capsid or a completely collapsed globular assembly. Although a structure consisting of 80 copies of VP1 does not fit with any structures possessing icosahedral symmetry, there is precedence in the literature about the P domain of VP1 forming assemblies with different symmetry (44).

Conclusions—The stability of the rNVLPs was investigated over a range of solution conditions using native ESI-MS. From these data, it was shown that upon alkaline treatment the rNVLPs disassemble, and the corresponding VP1 dimers that are released can reassemble into various VP1 oligomers based on the solution pH and ionic strength. Higher ionic strength and solution pH drive the assembly toward the formation of species consisting of 60 and 80 copies of VP1. It was also demonstrated that the capsid formation of the various VP1 oligomers was completely reversible. Structural analysis using AFM and IMMS of the fully assembled and large VP1 oligomers revealed that these particles possess a spherical geometry. This was to be expected for the fully assembled rNVLPs and for the VP_{60} species, but the precise structure of the $VP1_{80}$ remains intriguing. Overall, capsid (dis)assembly was found to be a very heterogeneous process and very sensitive to solution pH, ionic strength, and VP1 concentration. This work highlights the application of native ESI-MS to such analyses where the simultaneous detection of all oligomeric forms of a protein assembly can provide insights into the factors governing a process such as viral assembly.

* This work was supported, in whole or in part, by National Institutes of Health Grant PO1 AI057788 (to M. K. E.). This work was also supported by The Netherlands Proteomics Centre; the Natural Sciences and Engineering Research Council through a postdoctoral fellowship grant (to G. K. S.); The Netherlands Organisation for Scientific Research (NWO) through VENI Grant 700.58.402 (to E. v. D.), Aard-en Levenswetenschappen ECHO Grant 819.02.10 (to A. J. R. H.), a Chemische Watenschappen ECHO grant (to G. J. L. W.), and a Rubicon grant (to W. H. R.); and Robert Welch Foundation Grant Q1279 (to B. V. V. P.).

[S] This article contains supplemental Figs. S1 and S2 and Tables S1 and S2.

‡‡ To whom correspondence should be addressed. E-mail: a.j.r.heck@uu.nl.

REFERENCES

1. Atmar, R. L., and Estes, M. K. (2006) The epidemiologic and clinical importance of norovirus infection. *Gastroenterol. Clin. North Am.* **35,** 275–290, viii
2. Estes, M. K., Prasad, B. V., and Atmar, R. L. (2006) Noroviruses everywhere: has something changed? *Curr. Opin. Infect. Dis.* **19,** 467–474
3. Green, K. Y., Ando, T., Balayan, M. S., Berke, T., Clarke, I. N., Estes, M. K., Matson, D. O., Nakata, S., Neill, J. D., Studdert, M. J., and Thiel, H. J. (2000) Taxonomy of the caliciviruses. *J. Infect. Dis.* **181,** Suppl. 2, S322–S330
4. Jiang, X., Wang, M., Wang, K., and Estes, M. K. (1993) Sequence and genomic organization of Norwalk virus. *Virology* **195,** 51–61
5. Xi, J. N., Graham, D. Y., Wang, K. N., and Estes, M. K. (1990) Norwalk virus genome cloning and characterization. *Science* **250,** 1580–1583
6. Prasad, B. V., Rothnagel, R., Jiang, X., and Estes, M. K. (1994) 3-Dimensional structure of baculovirus-expressed Norwalk virus capsids. *J. Virol.* **68,** 5117–5125
7. Ausar, S. F., Foubert, T. R., Hudson, M. H., Vedvick, T. S., and Middaugh, C. R. (2006) Conformational stability and disassembly of Norwalk virus-like particles: effect of pH and temperature. *J. Biol. Chem.* **281,** 19478–19488
8. Bertolotti-Ciarlet, A., Crawford, S. E., Hutson, A. M., and Estes, M. K. (2003) The 3′ end of Norwalk virus mRNA contains determinants that regulate the expression and stability of the viral capsid protein VP1: a novel function for the VP2 protein. *J. Virol.* **77,** 11603–11615
9. Jiang, X., Wang, M., Graham, D. Y., and Estes, M. K. (1992) Expression, self-assembly, and antigenicity of the Norwalk virus capsid protein. *J. Virol.* **66,** 6527–6532
10. Bertolotti-Ciarlet, A., White, L. J., Chen, R., Prasad, B. V., and Estes, M. K. (2002) Structural requirements for the assembly of Norwalk virus-like particles. *J. Virol.* **76,** 4044–4055
11. Prasad, B. V., Hardy, M. E., Dokland, T., Bella, J., Rossmann, M. G., and Estes, M. K. (1999) X-ray crystallographic structure of the Norwalk virus capsid. *Science* **286,** 287–290
12. Heck, A. J. (2008) Native mass spectrometry: a bridge between interac-

tomics and structural biology. *Nat. Methods* **5,** 927–933
13. Ruotolo, B. T., Giles, K., Campuzano, I., Sandercock, A. M., Bateman, R. H., and Robinson, C. V. (2005) Evidence for macromolecular protein rings in the absence of bulk water. *Science* **310,** 1658–1661
14. Sharon, M., and Robinson, C. V. (2007) The role of mass spectrometry in structure elucidation of dynamic protein complexes. *Annu. Rev. Biochem.* **76,** 167–193
15. Uetrecht, C., Versluis, C., Watts, N. R., Roos, W. H., Wuite, G. J., Wingfield, P. T., Steven, A. C., and Heck, A. J. (2008) High-resolution mass spectrometry of viral assemblies: Molecular composition and stability of dimorphic hepatitis B virus capsids. *Proc. Natl. Acad. Sci. U.S.A.* **105,** 9216–9220
16. Kaddis, C. S., Lomeli, S. H., Yin, S., Berhane, B., Apostol, M. I., Kickhoefer, V. A., Rome, L. H., and Loo, J. A. (2007) Sizing large proteins and protein complexes by electrospray ionization mass spectrometry and ion mobility. *J. Am. Soc. Mass Spectrom.* **18,** 1206–1216
17. Uetrecht, C., Versluis, C., Watts, N. R., Wingfield, P. T., Steven, A. C., and Heck, A. J. (2008) Stability and shape of hepatitis B virus capsids in vacuo. *Angew. Chem. Int. Ed. Engl.* **47,** 6247–6251
18. Synowsky, S. A., van den Heuvel, R. H., Mohammed, S., Pijnappel, P. W., and Heck, A. J. (2006) Probing genuine strong interactions and post-translational modifications in the heterogeneous yeast exosome protein complex. *Mol. Cell. Proteomics* **5,** 1581–1592
19. van Duijn, E., Bakkes, P. J., Heeren, R. M., van den Heuvel, R. H., van Heerikhuizen, H., van der Vies, S. M., and Heck, A. J. (2005) Monitoring macromolecular complexes involved in the chaperonin-assisted protein folding cycle by mass spectrometry. *Nat. Methods* **2,** 371–376
20. Barrera, N. P., Isaacson, S. C., Zhou, M., Bavro, V. N., Welch, A., Schaedler, T. A., Seeger, M. A., Miguel, R. N., Korkhov, V. M., van Veen, H. W., Venter, H., Walmsley, A. R., Tate, C. G., and Robinson, C. V. (2009) Mass spectrometry of membrane transporters reveals subunit stoichiometry and interactions. *Nat. Methods* **6,** 585–587
21. Zhou, M., Sandercock, A. M., Fraser, C. S., Ridlova, G., Stephens, E., Schenauer, M. R., Yokoi-Fong, T., Barsky, D., Leary, J. A., Hershey, J. W., Doudna, J. A., and Robinson, C. V. (2008) Mass spectrometry reveals modularity and a complete subunit interaction map of the eukaryotic translation factor eIF3. *Proc. Natl. Acad. Sci. U.S.A.* **105,** 18139–18144
22. Taverner, T., Hernández, H., Sharon, M., Ruotolo, B. T., Matak-Vinkoviæ, D., Devos, D., Russell, R. B., and Robinson, C. V. (2008) Subunit architecture of intact protein complexes from mass spectrometry and homology modeling. *Acc. Chem. Res.* **41,** 617–627
23. Lorenzen, K., Vannini, A., Cramer, P., and Heck, A. J. (2007) Structural biology of RNA polymerase III: mass spectrometry elucidates subcomplex architecture. *Structure* **15,** 1237–1245
24. Hoaglund, C. S., Valentine, S. J., Sporleder, C. R., Reilly, J. P., and Clemmer, D. E. (1998) Three-dimensional ion mobility TOFMS analysis of electrosprayed biomolecules. *Anal. Chem.* **70,** 2236–2242
25. Siuzdak, G., Bothner, B., Yeager, M., Brugidou, C., Fauquet, C. M., Hoey, K., and Chang, C. M. (1996) Mass spectrometry and viral analysis. *Chem. Biol.* **3,** 45–48
26. Tito, M. A., Tars, K., Valegard, K., Hajdu, J., and Robinson, C. V. (2000) Electrospray time-of-flight mass spectrometry of the intact MS2 virus capsid. *J. Am. Chem. Soc.* **122,** 3550–3551
27. Morton, V. L., Stockley, P. G., Stonehouse, N. J., and Ashcroft, A. E. (2008) Insights into virus capsid assembly from non-covalent mass spectrometry. *Mass Spectrom. Rev.* **27,** 575–595
28. van den Heuvel, R. H., van Duijn, E., Mazon, H., Synowsky, S. A., Lorenzen, K., Versluis, C., Brouns, S. J., Langridge, D., van der Oost, J., Hoyes, J., and Heck, A. J. (2006) Improving the performance of a quadrupole time-of-flight instrument for macromolecular mass spectrometry. *Anal. Chem.* **78,** 7473–7483
29. Lorenzen, K., Versluis, C., van Duijn, E., van den Heuvel, R. H., and Heck, A. J. (2007) Optimizing macromolecular tandem mass spectrometry of large non-covalent complexes using heavy collision gases. *Int. J. Mass Spectrom.* **268,** 198–206
30. Sobott, F., Hernández, H., McCammon, M. G., Tito, M. A., and Robinson, C. V. (2002) A tandem mass spectrometer for improved transmission and analysis of large macromolecular assemblies. *Anal. Chem.* **74,** 1402–1407
31. Pringle, S. D., Giles, K., Wildgoose, J. L., Williams, J. P., Slade, S. E., Thalassinos, K., Bateman, R. H., Bowers, M. T., and Scrivens, J. H. (2007) An investigation of the mobility separation of some peptide and protein ions using a new hybrid quadrupole/travelling wave IMS/oa-ToF instrument. *Int. J. Mass Spectrom.* **261,** 1–12
32. Ruotolo, B. T., Benesch, J. L., Sandercock, A. M., Hyung, S. J., and Robinson, C. V. (2008) Ion mobility-mass spectrometry analysis of large protein complexes. *Nat. Protoc.* **3,** 1139–1152
33. van Duijn, E., Barendregt, A., Synowsky, S., Versluis, C., and Heck, A. J. (2009) Chaperonin complexes monitored by ion mobility mass spectrometry. *J. Am. Chem. Soc.* **131,** 1452–1459
34. de Pablo, P. J., Colchero, J., Gomez-Herrero, J., and Baro, A. M. (1998) Jumping mode scanning force microscopy. *Appl. Phys. Lett.* **73,** 3300–3302
35. Sader, J. E., Chon, J. W., and Mulvaney, P. (1999) Calibration of rectangular atomic force microscope cantilevers. *Rev. Sci. Instrum.* **70,** 3967–3969
36. Ivanovska, I. L., de Pablo, P. J., Ibarra, B., Sgalari, G., MacKintosh, F. C., Carrascosa, J. L., Schmidt, C. F., and Wuite, G. J. (2004) Bacteriophage capsids: tough nanoshells with complex elastic properties. *Proc. Natl. Acad. Sci. U.S.A.* **101,** 7600–7605
37. Felitsyn, N., Peschke, M., and Kebarle, P. (2002) Origin and number of charges observed on multiply-protonated native proteins produced by ESI. *Int. J. Mass Spectrom.* **219,** 39–62
38. Heck, A. J., and Van Den Heuvel, R. H. (2004) Investigation of intact protein complexes by mass spectrometry. *Mass Spectrom. Rev.* **23,** 368–389
39. White, L. J., Hardy, M. E., and Estes, M. K. (1997) Biochemical characterization of a smaller form of recombinant Norwalk virus capsids assembled in insect cells. *J. Virol.* **71,** 8066–8072
40. Harrison, S. C. (2001) The familiar and the unexpected in structures of icosahedral viruses. *Curr. Opin. Struct. Biol.* **11,** 195–199
41. Zlotnick, A., Aldrich, R., Johnson, J. M., Ceres, P., and Young, M. J. (2000) Mechanism of capsid assembly for an icosahedral plant virus. *Virology* **277,** 450–456
42. Rapaport, D. C. (2008) Role of reversibility in viral capsid growth: a paradigm for self-assembly. *Phys. Rev. Lett.* **101,** 186101
43. Uetrecht, C., Rose, R. J., van Duijn, E., Lorenzen, K., and Heck, A. J. (2010) Ion mobility mass spectrometry of proteins and protein assemblies. *Chem. Soc. Rev*. **39,** 1633–1655
44. Tan, M., Fang, P., Chachiyo, T., Xia, M., Huang, P., Fang, Z., Jiang, W., and Jiang, X. (2008) Noroviral P particle: structure, function and applications in virus-host interaction. *Virology* **382,** 115–123
45. Lorenzen, K., Olia, A. S., Uetrecht, C., Cingolani, G., and Heck, A. J. (2008) Determination of stoichiometry and conformational changes in the first step of the P22 tail assembly. *J. Mol. Biol.* **379,** 385–396